



The Piancaldoli meteorite: A forgotten primitive LL3.10 ordinary chondrite

Yves Marrocchi, Lydie Bonal, Jérôme Gattacceca, Laurette Piani, Pierre Beck, Richard Greenwood, Jolantha Eschrig, Anne Basque, Pasquale Mario Nuccio, Franco Foresta Martin

► To cite this version:

Yves Marrocchi, Lydie Bonal, Jérôme Gattacceca, Laurette Piani, Pierre Beck, et al.. The Piancaldoli meteorite: A forgotten primitive LL3.10 ordinary chondrite. *Meteoritics and Planetary Science*, 2020, 55 (8), pp.1924-1935. 10.1111/maps.13552 . hal-03009455

HAL Id: hal-03009455

<https://hal.univ-lorraine.fr/hal-03009455>

Submitted on 31 Aug 2021

HAL is a multi-disciplinary open access archive for the deposit and dissemination of scientific research documents, whether they are published or not. The documents may come from teaching and research institutions in France or abroad, or from public or private research centers.

L'archive ouverte pluridisciplinaire **HAL**, est destinée au dépôt et à la diffusion de documents scientifiques de niveau recherche, publiés ou non, émanant des établissements d'enseignement et de recherche français ou étrangers, des laboratoires publics ou privés.

The Piancaldoli meteorite: A forgotten primitive LL3.10 ordinary chondrite

Yves Marrocchi^{1,*}, Lydie Bonal², Jérôme Gattacceca³, Laurette Piani¹, Pierre Beck²,
Richard Greenwood⁴, Jolantha Eschrig², Anne Basque¹, Pasquale Mario Nuccio⁵,
Franco Foresta Martin^{6,7}

¹CRPG, CNRS, Université de Lorraine, UMR 7358, Vandoeuvre-lès-Nancy, 54501, France

²Institut de Planétologie et d'Astrophysique de Grenoble, Grenoble, France

³Aix-Marseille Univ, CNRS, IRD, Coll France, INRAE, CEREGE, Aix-en-Provence, France

⁴PSS, Open University, Walton Hall, Milton Keynes MK7 6AA, UK

⁵Full professor of Geochemistry and Volcanology, Università di Palermo, Italy

⁶Istituto Nazionale di Geofisica e Vulcanologia, Sezione di Palermo, 90146 Palermo, Italy

⁷Laboratorio Museo di Scienze della Terra, Ustica, Palermo, Italy

*Corresponding author: yvesm@crpg.cnrs-nancy.fr

26

27 **Abstract**

28 The Piancaldoli ordinary chondrite fell in northern Italy on 10 August 1968.
29 Preliminary studies led to its classification as a LL3.4 unequilibrated ordinary chondrite.
30 However, recent developments in classification procedures have prompted us to re-examine
31 its mineralogical, petrographic, spectroscopic, chemical, and isotopic features in a multi-
32 technique study. Raman spectra and magnetic properties indicate that Piancaldoli experienced
33 minimal thermal metamorphism, consistent with its high bulk hydrogen content and the Cr
34 contents of ferroan olivines in its type-II chondrules. In combination with findings of previous
35 studies, our data thus confirm the variability of Cr contents in ferroan olivines in type-II
36 chondrules as a proxy of thermal metamorphism. Furthermore, our results reveal that
37 Piancaldoli is less altered than previously reported and should be reclassified as **an** LL3.10
38 unequilibrated ordinary chondrite. Our results also imply that the bulk deuterium enrichment,
39 as observed in Piancaldoli (LL3.10), Bishunpur (LL3.15), and Semarkona (LL3.00), is a
40 specific signature of the most primitive unequilibrated ordinary chondrites. Based on our
41 results, we propose that, to date, Piancaldoli is the second least-altered unequilibrated
42 ordinary chondrite fall after Semarkona. This work reiterates the importance of meteorite
43 collections worldwide as fundamental resources for studying the formation conditions and
44 evolution our solar system.

45

46 **Keywords:** Ordinary chondrites, meteorite classification, thermal metamorphism, Piancaldoli

47

48

49

50

1. Introduction

On 26 April 1803, thousands of stones fell upon the small city of L'Aigle, France (~150 km west of Paris). At that time, the extraterrestrial nature of meteorites was not yet recognized and they were still considered to be ‘thunderstones’ resulting from atmospheric processes. The precise description of the L'Aigle fall by dozens of people and the unique nature of the recovered rocks led physicist Jean-Baptiste Biot to conclude their origin to be unambiguously extraterrestrial. The extraterrestrial origin of meteorites had already been proposed on the basis of meteor ballistic trajectories and chemical analyses performed by Ernst Florens Friedrich Chladni (see Marvin, 2010 for a review) and Edward Howard (Howard et al., 1802). Since these works, meteorites have been recognized as objects of scientific importance, and natural history museums worldwide have established invaluable meteorite collections. Despite the recent boom in space exploration, most of our current understanding of the conditions and chronology of the formation of the solar system has been established thanks to the meticulous work of meteorite collection and curation (Heck et al. 2019).

Over the past two decades, the number of meteorites reported to the Meteoritical Society has increased exponentially thanks to field trips organized to cold and hot deserts expressly to search for meteorites (e.g., Harvey, 2003; Gattacceca et al. 2011; Evatt et al. 2020). These harvests have enabled the characterization of some of the most primitive meteorites known so far, which are now available to the scientific community. However, meteorite finds are exposed to terrestrial weathering and contamination, which largely affect their primitive characteristics (Alexander 2017; Stephant et al. 2018; Vacher et al. 2020). For instance, Antarctic and Saharan samples are commonly affected by Na loss and/or metal alteration, and Antarctic samples by oxygen isotopic exchange with Antarctic water

(Alexander et al. 2018). Thus, as meteorite falls are collected before any significant terrestrial alteration can occur, they are of primary importance for deciphering the formation of the solar system.

In addition to terrestrial weathering, most chondrites experienced secondary alteration on their asteroidal parent bodies, resulting in changes to their primary texture, mineralogy, and chemical and isotopic compositions (Brearley 2006; Marrocchi et al. 2018). These petrographic and chemical modifications are the basis of petrologic type assignments (Van Schmus and Wood 1967) on a scale from 1 to 6, reflecting the progressive roles of low-temperature aqueous alteration (types 3 to 1) and thermal metamorphism (types 3 to 6). In theory, type-3 chondrites thus correspond to primitive materials that underwent minimal modifications after their agglomeration in the protoplanetary disk 4.56 Ga (Amelin et al., 2010). However, new classification procedures based on thermoluminescence (TL; Sears et al. 1980), chemical characteristics (e.g., Cr content in ferroan olivines in type-II chondrules; Grossman and Brearley 2005) and Raman spectroscopy (Bonal et al. 2006, 2007, 2016) permit the quantification of discrete variations among type-3 chondrites. Accordingly, type-3 chondrites are now subdivided into categories ranging from 3.00 to 3.9, with 3.00 being the most *primitive* extraterrestrial materials, virtually unchanged since their agglomeration in the disk.

Because these advances in the classification of minimally altered chondrites are relatively recent (Grossman and Brearley 2005; Bonal et al. 2006, 2016), many previously analyzed chondrites have not been characterized according to the new classification criteria nor studied in further detail after their initial classification. This is fundamental, however, as the identification of primitive chondrites with minimal parent-body alteration improves our understanding of the formation and evolution of solids in the protoplanetary disk. In particular, Al-Mg chronology requires the characterization of refractory inclusions and chondrules in

chondrites of petrologic subtypes ≤ 3.1 due to the fast self-diffusion of Mg in minerals and glassy mesostases (Kita and Ushikubo 2012; Van Orman et al. 2014; Marrocchi et al. 2019).

While vacationing in Sicily in 2018, the first author (YM) fortuitously met Franco Foresta Martin, a geologist and a journalist at the Italian national daily newspaper *Corriere della Sera*. He brought to my knowledge the history of the Piancaldoli meteorite that fell near Florence in northern Italy on 10 August 1968. A fireball was observed over Yugoslavia and central and northern Italy, followed by explosions accompanying the break-up of the meteorite. Three meteorite fragments totaling 13.1 g were found on the roof of a house in Piancaldoli. The Piancaldoli meteorite was first classified as a L3 chondrite (Carapezza and Nuccio 1971) before being reclassified as LL3 (Carapezza et al. 1975, 1976). Although no Raman or TL data were available for Piancaldoli, Rubin et al. (1982) proposed its reclassification as petrologic type 3.4 ± 0.2 based on silicate compositions. Consequently, Piancaldoli is listed as a LL3.4 ordinary chondrite in the Meteoritical Bulletin Database. Here we report a comprehensive description of Piancaldoli and show that its secondary thermal history was overestimated. Our results indicate that Piancaldoli is the second least-altered unequilibrated ordinary chondrite fall known to date.

2. Material and methods

2.1 Mineralogical and petrographic observations

We surveyed two sections of Piancaldoli: thin section USNM 5649 from the National Museum of Natural History, Smithsonian Institution (Washington D.C., USA) and a thick section prepared at the Centre de Recherches Pétrographiques et Géochimiques (CRPG-CNRS, Nancy, France) from a parent sample provided by the Dipartimento scienze della Terra e del Mare (Palermo, Italy). We also characterized a thin section of Semarkona (LL3.00; Grossman and Brearley, 2005; Muséum national d'Histoire naturelle, Paris, France)

and a thick section of Bishunpur (LL3.15; Grossman and Brearley, 2005; Muséum national d'Histoire naturelle, Paris, France) for comparison. The sections were imaged by scanning electron microscopy on a JEOL JSM-6510 equipped with a Genesis energy dispersive x-ray (EDX) detector at the CRPG using a 3 nA electron beam accelerated at 15 kV. The chemical compositions of olivine grains were quantified using a Cameca SXFive electron microprobe at the Université Pierre et Marie Curie (UPMC, Campus, Paris, France) using a 150 nA focused beam accelerated at 15 kV. We analyzed Na, Mg, Si, Al, K, Ca, Fe, Ti, Cr, and Mn in olivine grains. The high beam current allowed detection limits for silicates to be 100 ppm for Al, Ca, and Ti, 150 ppm for Mn and Si, and 200 ppm for Na, K, Cr, Fe, and Mg. The PAP software was used for matrix corrections.

2.2 Raman spectroscopy

Raman spectroscopy was performed at the Ecole Normale Supérieure de Lyon (Laboratoire de Géologie de Lyon – Terre, Planètes, Environnement, France) using a LabRam Raman spectrometer (Horiba Jobin-Yvon) equipped with a 600 gr/mm grating and a Spectra Physics Ar⁺ laser ($\lambda = 514$ nm). Because carbonaceous matter is sensitive to laser-induced heating and the Raman bands of polyaromatic carbonaceous matter are dispersive, we followed the analytical procedures of Bonal et al. (2016, summarized here) to avoid any laser alteration of the carbonaceous matter and to facilitate meaningful comparisons with reference meteorites from the literature. The laser was focused through a 100× objective to obtain a ~2 μ m spot size. The power on the sample was 500 μ W. Each acquisition comprised two 30-s integrations that were averaged to make the final spectrum. Spectra were acquired under atmospheric conditions over the wavenumbers 500–2,200 cm^{-1} , covering the first-order carbon bands. Raman spectra of carbonaceous matter in the matrix of Piancaldoli were obtained both on isolated matrix fragments (50 spectra) and *in situ* in the thick section

prepared at the CRPG (32 spectra). Around 30 matrix fragments (typical apparent diameter around 30 μm) were manually selected from a gently crushed raw piece of Piancaldoli (initial sample of 50 mg) according to their color and texture under a binocular microscope. The selected matrix fragments were pressed between two glass slides that served as the substrate for the Raman analyses. The G and D bands were fitted with Breit-Wigner-Fano and Lorentzian profiles, respectively, to retrieve spectral parameters. We compared the width (full width at half maximum) of the D band (FWHM_D , cm^{-1}) and its intensity relative to that of the G band (I_D/I_G) to those of reference samples as these spectral parameters are the most sensitive to the maturity range of type-3 chondrites (e.g., Bonal et al., 2016).

2.3 Infrared spectroscopy

Infrared (IR) spectra were obtained with a Bruker HYPERION 3000 infrared microscope at the Institut de Planétologie et d'Astrophysique de Grenoble (IPAG, Grenoble, France). The IR beam was focused through a 15 \times objective to a typical spot size on the sample of $40 \times 40 \mu\text{m}^2$. Spectra were acquired at 4 cm^{-1} spectral resolution with a MCT detector cooled with liquid nitrogen. Particular care was devoted to sample preparation, which is critical in IR microspectroscopy. Samples must be sufficiently thin ($<100 \mu\text{m}$) and their surfaces flat and parallel to avoid absorption-band saturation and scattering artifacts, respectively (Raynal et al. 2000). Small matrix fragments (30–50 μm) were selected under a binocular microscope and crushed between two diamond windows for analyses in the 4000–650 cm^{-1} spectral range. The diamond windows were loaded into an environmental cell, designed and built at IPAG, capable of achieving temperatures up to 300 $^\circ\text{C}$ under primary or secondary dynamic vacuum (10^{-4} to 10^{-7} mbar). Optical access is via both sides of the cell through KBr windows, enabling measurements in transmission mode. Samples were progressively heated and analyzed at 20, 100, and 300 $^\circ\text{C}$ for 1 hour at each temperature.

The transmission spectra were automatically converted to absorbance ($A = -\log (T/T_0)$, where T_0 and T are the background and sample transmittance, respectively). To remove interferences and scattering effects, a spline baseline was calculated and subtracted from the raw data. The resulting spectra were normalized to the intensity of the silicate Si-O stretching band (1000 cm^{-1}) at $10 \text{ }\mu\text{m}$ thickness, which does not evolve over the temperature range of the measurements. Reflectance spectra were obtained on powdered fragments of Piancaldoli using the SHADOWS instrument (Potin et al., 2018). Spectra were normalized to spectralonTM and infragoldTM and measured under standard mode.

2.4 Magnetic properties

Hysteresis measurements were performed on a 122-mg bulk (matrix + chondrules) fragment of Piancaldoli with a Princeton Micromag vibrating sample magnetometer with a maximum applied field of 1 T and a sensitivity of $\sim 5 \times 10^{-9} \text{ A m}^2$. We analyzed hysteresis loops to obtain the ratio of saturation remanent magnetization (M_{RS}) to saturation magnetization (M_S) and the coercive force (B_C). M_S was determined by correcting the hysteresis loop for the high-field susceptibility determined by a linear fit of the hysteresis loops for applied fields $> 0.9 \text{ T}$. Remanent coercive force (B_{CR}) was determined by back-field experiments performed with the magnetometer. The coercivity spectrum was estimated from the derivative of the isothermal remanent magnetization by stepwise measurements using the magnetometer. The evolution of low field magnetic susceptibility at low temperature was studied using an Agico MFK1 apparatus equipped with a CSL cryostat. All magnetic measurements were performed at the Centre Européen de Recherche et d'Enseignement des Géosciences de l'Environnement (Aix-en-Provence, France).

2.5 Hydrogen isotopes

Hydrogen concentrations and isotopic compositions were measured using the Thermo Scientific EA IsoLink - DeltaV IRMS System at the CRPG according to the procedure detailed in Lupker et al. (2012), which we summarize here. A small piece of the meteorite was crushed into powder and two aliquots (5.97 and 7.82 mg, respectively) were loaded into tin capsules and degassed at 120 °C under vacuum for 48 h to minimize the contribution of adsorbed atmospheric water (Lupker et al. 2012; Vacher et al. 2016, 2020). Hydrogen isotopic compositions are expressed relative to that of Standard Mean Ocean Water (SMOW, $D/H_{SMOW} = 155.76 \times 10^{-6}$) as $\delta D [‰] = [(D/H_{sample} / D/H_{SMOW}) - 1] \times 1,000$. Reproducibilities estimated from reference materials are better than 10% (2σ) for H concentration and 0.5×10^{-6} for D/H (or 5‰ for δD).

2.6 Oxygen isotopes

High-precision oxygen isotopic measurements were performed at the Open University (Milton Keynes, UK) using an infrared laser-assisted fluorination system (Miller et al., 1999; Greenwood et al., 2017). Two individual analyses of whole rock chips of Piancaldoli were undertaken, with each replicate having a mass of about 2 mg. After fluorination, the O_2 released was purified by passing through two cryogenic nitrogen traps and over a bed of heated KBr. O_2 analyses were performed using a MAT 253 dual inlet mass spectrometer. Analytical precision (2σ), based on replicate analyses of an internal obsidian standard, is $\pm 0.053 ‰$ for $\delta^{17}O$, $\pm 0.095 ‰$ for $\delta^{18}O$ and $\pm 0.018 ‰$ for $\Delta^{17}O$ (Starkey et al., 2016). Oxygen isotopic analyses are reported in standard δ notation, where $\delta^{18}O$ has been calculated as: $\delta^{18}O = [(^{18}O/^{16}O_{sample}/^{18}O/^{16}O_{ref.}) - 1] \times 100$ and similarly for $\delta^{17}O$ using the $^{17}O/^{16}O$ ratio. $\Delta^{17}O$, which represents the deviation from the terrestrial fractionation line, has been calculated as:

$\Delta^{17}\text{O} = \delta^{17}\text{O} - 0.525 \times \delta^{18}\text{O}$ in order to compare our results with those obtained by Clayton et al (1991).

3. Results

3.1 Petrographic overview

The Piancaldoli sections contain abundant chondrules (Figs. 1, 2) and chondrule fragments (Fig. 3) in an optically dark matrix. Type-I chondrules (characterized by abundant Fe-Ni metal beads, FeO-poor silicates and volatile element depletion) are predominantly olivine-rich and relatively homogeneous (Fig. 2A), whereas type-II chondrule (characterized by FeO-rich silicates and more chondritic abundances of volatile elements) are compositionally variable with normally zoned and relict, Mg-rich, olivine grains (Villeneuve et al., 2020; Fig. 2B). Some ferroan olivine grains show igneous zoning profiles, with rims enriched in Cr (Fig. 4), and chromite exsolutions are commonly observed in type-II chondrule olivines (Fig. 5). Although some type-II chondrules show devitrified mesostases, both types are characterized by well-preserved glassy mesostases (Figs. 2–4) with no specific evidence of aqueous alteration. Dusty olivine grains were observed in about 5% of 350 observed chondrules. Opaque mineral assemblages are rounded and occur predominantly along chondrule exteriors, but also rarely within the interiors of some chondrules (Fig. 1). Ferroan olivines in type-II chondrules of Piancaldoli contain 0.2–0.5 wt.% Cr_2O_3 , averaging 0.36 ± 0.20 wt.% Cr_2O_3 (1σ , Fig. 6, Table S1); those of Semarkona and Bishunpur contain 0.45 ± 0.11 and 0.23 ± 0.13 wt.% Cr_2O_3 , respectively (Fig. 6).

3.2 Raman and Infrared spectral characteristics

Every Raman spectrum obtained of the Piancaldoli matrix exhibits the D and G bands, indicating the presence of polyaromatic carbonaceous matter. We obtained mean values of

FWHM_D (cm⁻¹) = 173.4 ± 20.2 and $I_D/I_G = 0.912 \pm 0.089$ for *in-situ* thin-section analyses ($n = 32$) and FWHM_D (cm⁻¹) = 159.2 ± 37.8 and $I_D/I_G = 0.996 \pm 0.145$ for matrix fragments ($n = 50$; the errors reflecting the variable structural order of the polyaromatic carbonaceous matter).

These spectral parameters are thus variable throughout Piancaldoli: the structural order of the polyaromatic carbonaceous matter in the CRPG section of Piancaldoli reflects a metamorphic grade similar to that of Bishunpur (LL3.15), whereas the spectral parameters obtained for the matrix fragments are more dispersed and tend to reflect a slightly higher metamorphic grade (Fig. 7). This discrepancy might be explained by the brecciated nature of Piancaldoli (discussed in section 4).

The presence of aliphatic bands in the 2800–3000 cm⁻¹ range of IR spectra (Fig. 8) confirms our manual selection of matrix fragments because the matrix is the only petrographic component containing organics in chondrites. These IR spectra mostly exhibit bands related to Si-O stretching around 1000 cm⁻¹, indicating olivine to be the dominant silicate. The stretching mode of molecular water is poorly visible at ~3400 cm⁻¹, and the OH⁻ band at ~3670 cm⁻¹ is absent (Fig. 8).

The reflectance spectrum obtained for Piancaldoli presents the two typical absorption bands at 1 and 2-μm diagnostic of Fe-bearing silicates (olivine + pyroxene). The shape bands, in particular the reflectance maxima around 1.6 μm, is typical of LL chondrites (Fig 9). However, the depth of the two bands is lower than typical ordinary chondrites, which is likely related to the unequilibrated nature of the sample. The visible reflectance at 550 nm is lower than type 4-6 ordinary chondrites, and in low-side of the range of value measured for type 3 ordinary chondrites.

3.3 Magnetic properties

The hysteresis properties of the bulk Piancaldoli fragment are $M_S = 6.79 \text{ A m}^2/\text{kg}$, $M_{RS} = 0.216 \text{ A m}^2/\text{kg}$, $B_C = 9.02 \text{ mT}$, and $B_{CR} = 62.8 \text{ mT}$, in agreement with observed values for LL3 chondrite falls (Gattacceca et al. 2014). The M_S value indicates a metal content similar to other LL3 chondrites. The coercivity spectrum of Piancaldoli (Fig. 10) is difficult to fit with a typical combination of log-normally distributed components, and is notably shifted toward low coercivities compared to other LL chondrite falls, including LL3 chondrites. In particular, the absence of a peak in the high coercivity range ($>500 \text{ mT}$) precludes the presence of ordered tetrataenite in cloudy zone microstructures of zoned taenite (Gattacceca et al. 2014). Such microstructures form only by the cooling of Fe-Ni metal from above 320°C at cooling rates slower than $\sim 1000^\circ\text{C}/\text{Myr}$ (Gattacceca et al. 2014; Maurel et al. 2019) and can be disordered by impact-induced thermal events at or above shock stage S3/S4 (Gattacceca et al. 2014). In the case of Piancaldoli (shock stage S1), the absence of ordered tetrataenite constrains the peak metamorphism temperature to $<320^\circ\text{C}$. LL chondrites with broadly similar coercivity spectra include Bishunpur, Krymka, and Chainpur, although Piancaldoli has the lowest coercivities. Conversely, Vicencia (LL3) and all other equilibrated LL chondrites have high-coercivity components attributable to ordered tetrataenite in the cloudy zone structure (Fig. 10). It is therefore likely that the classification of Vicencia as LL3.2 (Keil et al. 2015) should be revised to a higher petrologic subtype, consistent with the observed Raman spectral parameters (see their Fig. 8, and Fig. 7 herein). Indeed, Vicencia appears to be more metamorphosed than Chainpur (LL3.4) and less than Tieschitz (H/L3.6).

The low temperature magnetic measurements performed on Piancaldoli do not reveal a Verwey transition at 120K that would indicate the presence of magnetite. Magnetite has been detected through low temperature magnetic measurements in a few primitive LL3 falls, such as Semarkona and Krymka (Keil et al., 2015), and through petrographic observation in, e.g.,

Semarkona (Hutchison et al., 1987). The absence of the Verwey transition in Piancaladoli confirms the absence of significant aqueous alteration.

3.4 H and O isotopes

The two analyzed aliquots of Piancaldoli contain 0.124 and 0.127 wt.% H, equivalent to 1.12 and 1.14 wt.% H₂O, respectively, and have respective D/H values of 193.2×10^{-6} ($\delta D = -57.7\text{‰}$) and 187.8×10^{-6} ($\delta D = -57.6\text{‰}$). These values are broadly typical of mildly metamorphosed LL3 chondrites (Robert et al. 1979; McNaughton et al. 1982; Yang and Epstein 1983; Alexander et al. 2012; Vacher et al. 2020). Although the hydrogen concentrations are on the higher end of those measured for LL3 chondrites similar to Semarkona (~0.04–0.12 wt.% H), the D/H ratios are intermediate among the range observed for LL3 chondrites (158×10^{-6} to 505×10^{-6} ; Fig. 11).

The results of oxygen isotope measurement of Piancaldoli are plotted in Fig. 12. The two individual analyses show consistent results with $\delta^{18}\text{O} = 5.16 \pm 0.21 \text{‰}$ (2σ) and $\delta^{17}\text{O} = 3.63 \pm 0.18 \text{‰}$ (2σ). Compared to other ordinary chondrites, Piancaldoli plots at the edge of the LL chondrite field with a relatively low $\Delta^{17}\text{O}$ value of $0.95 \pm 0.08 \text{‰}$ (2σ ; Fig. 12).

4. Discussion

The Piancaldoli chondrite contains sharply defined type-I and type-II chondrules (Fig. 2) with a mean apparent diameter of $901 \pm 445 \text{ }\mu\text{m}$, and a median apparent diameter of $804 \text{ }\mu\text{m}$ ($n=352$). Rubin et al. (1982) described a Piancaldoli clast with ~100 radial-pyroxene microchondrules 0.2–64 μm in apparent diameter. Chondrule olivine and pyroxene crystals show heterogeneous compositions with (i) olivine varying between 66 and 98 mol% of forsterite and (ii) pyroxene ranging from 2 to 24 mol% of ferrosilite (Carapezza et al., 1976; Rubin et al., 1982). The chemical composition of Piancaldoli is typical of LL ordinary chondrites with

FeO/SiO₂ = 0.48, SiO₂/MgO 1.62, and Fe⁰/Fe_{tot} = 0.12 (Carapezza et al. 1976; Wasson and Kallemeyn, 1988). In addition, the chemical compositions of the fine-grained opaque matrix and the whole rock were used to propose that Piancaldoli is an unequilibrated LL ordinary chondrite of petrologic type 3.4 ± 0.2 (Carapezza et al. 1976; Rubin et al. 1982). However, all data collected herein indicate that Piancaldoli is more primitive than this estimation. Thus, in this section, we (i) assess the extent of thermal alteration experienced by Piancaldoli and (ii) propose a new classification.

The distribution of Cr contents in ferroan olivines in type-II chondrules is considered a proxy of incipient thermal metamorphism. We obtained a mean value of 0.36 ± 0.19 wt.% Cr₂O₃ (Fig. 6; Table S1) for type-II chondrule olivines in Piancaldoli, and our measurements of those in Semarkona and Bishunpur during the same analytical session are in good agreement with previous reports (Grossman and Brearley 2005; Fig. 6). This suggests that Piancaldoli experienced minimal thermal metamorphism corresponding to petrologic type 3.10 (Fig. 6; Grossman and Brearley 2005), supported by the occurrence of igneous Cr zoning patterns (i.e., rims enriched in Cr) in some type-II chondrule olivines (Fig. 4). Such primary textures are extremely sensitive to thermal metamorphism as they are replaced by complex, subparallel, needle-like exsolutions of Cr-rich phases (likely chromite; Fig. 5) upon heating (Grossman and Brearley 2005). As the separation of Cr-rich phases from FeO-rich olivine grains is nearly complete by petrologic type 3.2 (Grossman and Brearley 2005), the observed Cr zonings in Piancaldoli olivine are a strong argument in favor of Piancaldoli's primitive nature.

Tetrataenite dominates the magnetic properties of all but the most primitive LL chondrites (and those that experienced shock stage S4 or greater). The absence of tetrataenite revealed by the magnetic properties of Piancaldoli sets it among the most primitive LL chondrites and constrains the peak metamorphic temperature to <320 °C. This low degree of

thermal metamorphism is supported by the structural order of the polyaromatic carbonaceous matter in Piancaldoli. Indeed, the Raman spectral parameters of polyaromatic carbon bands of Piancaldoli are comparable with those of Bishunpur (LL3.15; Fig. 7). Interestingly, spectra obtained on matrix fragments selected from a piece of bulk Piancaldoli exhibit a wider spectral variability, and, on average, a higher maturity (higher I_D/I_G and lower FWHM_D , Fig. 7). Therefore, some parts of Piancaldoli appear to have experienced a higher peak metamorphic temperature consistent with a petrologic type closer to 3.4. This variable metamorphic grade is consistent with previous petrographic observations and could be related to the brecciated nature of Piancaldoli (as attested by the presence of light- and dark-colored matrix domains in section USNM 5640; Rubin et al. 1982). Indeed, the fine exsolutions of Cr-rich phases commonly observed in Piancaldoli (Fig. 5) suggest that it is more altered than Semarkona, in which such textures are absent (Grossman and Brearley 2005).

Infrared spectra of Piancaldoli's matrix indicate, if not the absence, the really low abundance of secondary hydrated minerals, and thus that Piancaldoli did not experience significant aqueous alteration. This is in contrast to the matrix of Semarkona (LL3.00), which clearly contains hydrated material, most likely smectite (Alexander et al. 1989; Quirico et al. 2003).

The hydrogen content and isotopic composition of Piancaldoli show important similarities with the two least-altered ordinary chondrite falls, Semarkona and Bishunpur (Fig. 11). The hydrogen content of Piancaldoli (~ 0.125 wt.%) is among the highest observed in ordinary chondrites (despite the removal of adsorbed atmospheric water before measurement in our methodology; Vacher et al. 2016, 2020) and is similar to the highest values reported for Semarkona (0.12 wt.% H; Alexander et al. 2012), further indicating that Piancaldoli experienced minimal thermal metamorphism, which would have resulted in hydrogen loss (Fig. 11). As neither phyllosilicates nor magnetite were observed in Piancaldoli, the H budget

is likely controlled by: (i) insoluble organic matter and (ii) chondrules (silicates and glassy mesostases). However, a detailed TEM study should be performed to clearly rule out the presence of phyllosilicates (Hutchison et al., 1987). Although enriched in deuterium compared to more metamorphosed ordinary chondrites, the rather low D/H signature of Piancaldoli relative to Semarkona and Bishunpur may be a consequence of the D/H heterogeneities observed among unequilibrated LL chondrites. Indeed, D/H values reported for Semarkona and Bishunpur are highly heterogeneous, ranging from 393 to 609×10^{-6} and from 253 to 504×10^{-6} , respectively (McNaughton et al. 1982; Yang and Epstein 1983; Alexander et al. 2012; Piani et al. 2015). Therefore, it seems that heterogeneous H isotopic compositions can be taken as an argument for the primitive nature of unequilibrated LL ordinary chondrites.

5. Concluding remarks

We studied the Piancaldoli chondrite via scanning electron microscopy, electron microprobe analyses, hydrogen and oxygen isotopic analyses, magnetic measurements, and Raman and IR spectroscopy. Characteristics of the Raman spectra and magnetic properties of Piancaldoli are consistent with its primitive nature as inferred from the variability of Cr contents in ferroan olivines in type-II chondrules. Furthermore, the high bulk H content of Piancaldoli indicates that it experienced only minimal thermal metamorphism. Our petrographic and chemical results therefore suggest that Piancaldoli should be reclassified as a LL3.10 unequilibrated ordinary chondrite, rather than a LL3.4 as previously proposed. We further suggest that the deuterium observed in Piancaldoli, Bishunpur, and Semarkona are specific signatures of the most primitive unequilibrated LL ordinary chondrites. Our results thus demonstrate that (i) Piancaldoli is the second least-altered unequilibrated ordinary chondrite fall after Semarkona,

400 and (ii) primitive meteorites are most likely sitting, unstudied, in meteorite collections
401 worldwide.

402

403

404

405

406

407

408

409

410

411

412

413

414

415

416

417

418

419

420

421

422

423

424

Acknowledgments

We thank Colette Guilbaud, Michel Fialin, Nicolas Rividi, Maxime Piralla, Lionel G. Vacher, and Thomas Rigaudier for their assistance during sample preparation and analysis. We thank Ashley King and Tim Gregory for helpful reviews and Timothy Jull for editorial handling. This is CRPG-CNRS contribution #2732.

Figure captions

Fig. 1: Composite back-scattered electron images of Piancaldoli: (A) USNM 5649 and (B) Piancaldoli-CRPG.

Fig. 2: Back-scattered electron images of representative (A) type-I and (B) type-II chondrules with well-preserved mesostases.

Fig. 3: Back-scattered electron image of a fish-shaped chondrule fragment.

Fig. 4: EDX maps of (A) Si + Mg and (B) Cr in euhedral ferroan olivine grains in a type-II chondrule of Piancaldoli. Olivine rims are enriched in Cr, representing an igneous zoning profile.

Fig. 5: Back-scattered electron image of a ferroan olivine grain in a type-II chondrule showing complex, subparallel, needle-like exsolutions of a Cr-rich phase (likely chromite).

Fig. 6: Standard deviation on Cr_2O_3 content *versus* mean Cr_2O_3 content of ferroan olivines in type-II chondrules in Piancaldoli compared to Semarkona and Bishunpur (data from this study and Grossman and Brearley, 2005). Piancaldoli lies between Semarkona and Bishunpur, suggesting it is of petrologic subtype 3.10.

Fig. 7: Spectral parameters (FWHMD vs. ID/IG, averages and one standard deviations) of Raman bands attributed to carbonaceous materials in Piancaldoli compared to other

meteorites (see Bonal et al., 2016). Data for Vicencia (LL), Axtell (CV3) and ALHA 77307 (CO3) are also reported (see section 3.3).

Fig. 8: Baseline-corrected transmission IR spectra (normalized to the height of the Si-O band at 1000 cm^{-1}) of matrix fragments of Piancaldoli, acquired at $20\text{ }^{\circ}\text{C}$ under dynamic vacuum. A vertical offset was applied to ease comparison. Notably, the water band is very weak and olivine is the dominant silicate.

Fig. 9: Left: Reflectance spectra of Piancaldoli powder compared to average ordinary chondrites spectra from the RELAB database. Spectra were normalized at 550 nm . Right: Reflectance value at 550 nm of Piancaldoli compared to ordinary chondrites, as a function of petrographic type.

Fig. 10: Coercivity spectra, i.e., the derivative of the isothermal remanent magnetization, IRM, (normalized to saturation remanence) as a function of the acquisition field, of LL chondrite falls. The petrologic types and masses of each chondrite is indicated.

Fig. 11: Hydrogen content (reported as $1/H_{\text{wt}\%}$) and isotopic composition of Piancaldoli compared to H, L, and LL ordinary chondrites. The hydrogen concentration of Piancaldoli plots in the range of poorly metamorphosed LL3 chondrites. Error bars represent 1σ standard deviations for chondrites having multiply reported hydrogen compositions (data from Robert et al. 1979; McNaughton et al. 1982; Yang and Epstein 1983; Alexander et al. 2012; Vacher et al. 2020).

Fig. 12: The oxygen isotopic composition of Piancaldoli compared to H, L, and LL ordinary chondrites (data from Clayton et al., 1991 and Greenwood et al., 2020) . Piancaldoli plots at the edge of the LL chondrite field with a relatively low $\Delta^{17}\text{O}$ value.

References

- Alexander C. M. O'D., Barber D. J., and Hutchison R. 1989. The microstructure of Semarkona and Bishunpur. *Geochimica et Cosmochimica Acta* 53:3045–3057.
- Alexander C. M. O'D., Bowden R., Fogel M. L., Howard K. T., Herd C. D. K., and Nittler L. R. 2012. The Provenances of Asteroids, and Their Contributions to the Volatile Inventories of the Terrestrial Planets. *Science* 337:721–723.
- Alexander C. M. O'D. 2017. The origin of inner Solar System water. *Philosophical Transactions of the Royal Society A: Mathematical, Physical and Engineering Sciences* 375:20150384–20.
- Alexander C. M. O'D., McKeegan K. D., and Altwegg K. 2018. Water Reservoirs in Small Planetary Bodies: Meteorites, Asteroids, and Comets. *Space Science Review* 214:36.
- Amelin Y., Kaltenbach A., Iizuka T., Stirling C. H., Ireland T. R., Petaev M., Jacobsen S. B. 2010. U–Pb chronology of the Solar System's oldest solids with variable $^{238}\text{U}/^{235}\text{U}$. *Earth and Planetary Science Letters* 300:343–350.
- Bonal L., Quirico E., Bourot-Denise M., and Montagnac G. 2006. Determination of the petrologic type of CV3 chondrites by Raman spectroscopy of included organic matter. *Geochimica et Cosmochimica Acta* 70:1849–1863.
- Bonal L., Bourot-Denise M., Quirico E., Montagnac G., and Lewin E. 2007. Organic matter and metamorphic history of CO chondrites. *Geochimica et Cosmochimica Acta* 71:1605–1623.
- Bonal L., Quirico E., Flandinet L., and Montagnac G. 2016. Thermal history of type 3 chondrites from the Antarctic meteorite collection determined by Raman spectroscopy of their polyaromatic carbonaceous matter. *Geochimica et Cosmochimica Acta* 189:312–337.

546 Brearley A. J. 2006. The action of water. In *Meteorites and the early solar system II*, edited by
 547 Laurretta D. S. and McSween H. Y. Tucson, Arizona: The University of Arizona Press. pp.
 548 587–624.

549 Carapezza M., and Nuccio M. 1971. The Piancaldoli meteorite. *Meteoritics* 6, 255.

550 Carapezza M., Nuccio P.M., and Valenza M. 1975. Piancaldoli meteorite: chemistry and
 551 mineralogy. *Meteoritics* 10, 369.

552 Carapezza M., Nuccio P.M., and Valenza M. 1976. Piancaldoli meteorite: chemistry,
 553 mineralogy and petrology. *Meteoritics* 11, 165.

554 Clayton R. N., Mayeda T. K., and Goswami J. N. 1991. Oxygen isotope studies of ordinary
 555 chondrites. *Geochimica et Cosmochimica Acta* 55:2317–2337.

556 Evatt G. W., Smedley A. R. D., Joy K. H., Hunter L., Tey W. H., Abrahams I. D., and Gerrish
 557 L. 2020. The spatial flux of Earth’s meteorite falls found via Antarctic data. *Geology* 48:
 558 G46733.1.

559 Gattacceca J. et al. 2011. The densest meteorite collection area in hot deserts: The San Juan
 560 meteorite field (Atacama Desert, Chile). *Meteoritics & Planetary Science* 46:1276–1287.

561 Gattacceca J., Suavet C., Rochette P., Weiss B.P., Winklhofer M., Uehara M., Friedrich J.
 562 2014. Metal phases in ordinary chondrites: magnetic hysteresis properties and
 563 implications for thermal history. *Meteoritics and Planetary Science*, 49:652-676.

564 Greenwood R.C., Burbine T.H., and Franchi I.A. 2020. Linking asteroids and meteorites to the
 565 primordial planetesimals population. *Geochimica et Cosmochimica Acta* 277:377-406.

566 Grossman J. N., and Brearley A. J. 2005. The onset of metamorphism in ordinary and
 567 carbonaceous chondrites. *Meteoritics & Planetary Science* 40:87–122.

568 Harvey R. 2003. The Origin and Significance of Antarctic Meteorites. *Geochemistry* 63:93-
 569 147.

570 Heck P. R. et al. 2019. Best practices for the use of meteorite names in publications.
 571 *Meteoritics & Planetary Science* 54:1397–1400.

572 Howard, E.C., Bournon, J.-L.Comte De, 1802. Experiments and observations on cer- tain
 573 stony and metalline substances, which at different times are said to have fallen on the Earth.
 574 *Philos. Trans. R. Soc. Lond.* 92:168–175.

575 Hutchison R., Alexander C. M. O'D., and Barber D. J. 1987. The Semarkona meteorite: first
 576 occurrence of smectite in an ordinary chondrites and its implications. *Geochimica et*
 577 *Cosmochimica Acta* 51:1875-1882.

578 Keil K. et al. 2015. The Vicência meteorite fall: A new unshocked (S1) weakly
 579 metamorphosed (3.2) LL chondrite. *Meteoritics & Planetary Science* 50: 1089–1111.

580 Kita N. T., and Ushikubo T. 2012. Evolution of protoplanetary disk inferred from ^{26}Al
 581 chronology of individual chondrules: Disk evolution and ^{26}Al chronology of chondrules.
 582 *Meteoritics & Planetary Science* 47:1108–1119.

583 Lupker M. et al. 2012. Predominant floodplain over mountain weathering of Himalayan
 584 sediments (Ganga basin). *Geochimica et Cosmochimica Acta* 84:410–432.

585 Marrocchi Y., Bekaert D. V., and Piani L. 2018. Origin and abundance of water in
 586 carbonaceous asteroids. *Earth and Planetary Science Letters* 482:23–32.

587 Marrocchi Y., Villeneuve J., Jacquet E., Piralla M., and Chaussidon M. 2019. Rapid
 588 condensation of the first Solar System solids. *Proceedings of the National Academy of*
 589 *Sciences of the United States of America* 116:23461–23466.

590 Marvin U.B. 2007. Ernst Florens Friedrich Chladni (1756-1827) and the origins of modern
 591 meteorite research. *Meteoritics & Planetary Science* 42:B3-B68.

592 Maurel C., Weiss B. P., Bryson J. F. J. 2019. Meteorite cloudy zone formation as a
 593 quantitative indicator of paleomagnetic field intensities and cooling rates on planetesimals.
 594 *Earth and Planetary Science Letters* 513:166-175.

595 McNaughton N. J., Fallick A. E., and Pillinger C. T. 1982. Deuterium enrichments in type 3
596 ordinary chondrites. *Journal of Geophysical Research* 87:A297.

597 Miller M. F., Franchi I. F., Sexton A. S. and Pillinger C. T. 1999. High precision $\delta^{17}\text{O}$
598 isotope measurements of oxygen from silicates and other oxides: methods and applications.
599 *Rapid Communication in Mass Spectrometry* 13:1211–1217.

600 Piani L., Robert F., and Remusat L. 2015. Micron-scale D/H heterogeneity in chondrite
601 matrices: A signature of the pristine solar system water? *Earth and Planetary Science*
602 *Letters* 415:154–164.

603 Potin S., Brissaud O., Beck P., Schmitt B., Magnard Y., Correia J.-J., Rabou P., and Jocu L.
604 2018. SHADOWS: a spectro-gonio radiometer for bidirectional reflectance studies of dark
605 meteorites and terrestrial analogs: design, calibrations, and performances on challenging
606 surfaces. *Applied Optics* 57:8279.

607 Quirico E., Raynal P.-I., Bourot-Denise M. 2003. Metamorphic grade of organic matter in six
608 unequilibrated ordinary chondrites. *Meteoritics & Planetary Science* 38:795-811.

609 Raynal P.-I., Quirico E., Borg J., Deboffle D., Dumas P., d 'Hendecourt L., Bibring J.-P., and
610 Langevin Y. 2000. Synchrotron infrared microscopy of micron-sized extraterrestrial grains.
611 *Planetary and Space Science* 48:1329–1339.

612 Robert F, Merlivat L, and Javoy M. 1979. Deuterium concentration in the early Solar System:
613 hydrogen and oxygen isotope study. *Nature* 282:785–789.

614 Rubin A. E., Scott E.R.D, and Keil K. 1982. Microchondrule-bearing clast in the Piancaldoli
615 LL3 meteorite: a new kind of type 3 chondrite and its relevance to the history of
616 chondrules. *Geochimica et Cosmochimica Acta* 46:1763–1776.

617 Sears D. W., Grossman J. N., Melcher C. L., Ross L. M., and Mills A. A. 1980. Measuring
618 metamorphic history of unequilibrated ordinary chondrites. *Nature* 287:791–795.

- Stephant A., Garvie L. A. J., Mane P., Hervig R., and Wadhwa M. 2018. Terrestrial exposure of a fresh Martian meteorite causes rapid changes in hydrogen isotopes and water concentrations. *Scientific Reports* 8:12385.
- Vacher L. G., Marrocchi Y., Verdier-Paoletti M. J., Villeneuve J., and Gounelle M. 2016. Inward radial mixing of interstellar water ices in the solar protoplanetary disk. *The Astrophysical Journal Letters* 827:1–6.
- Vacher L.G., Piani L., Rigaudier T., Thomassin D., Florin G., Piralla M., and Marrocchi Y. (2020). Hydrogen in chondrites: Influence of parent body alteration and atmospheric contamination on primordial components. *Geochimica et Cosmochimica Acta* 281:53-66.
- Van Orman J. A., Cherniak D. J., and Kita N. T. 2014. Magnesium diffusion in plagioclase: Dependence on composition, and implications for thermal resetting of the ^{26}Al – ^{26}Mg early solar system chronometer. *Earth and Planetary Science Letters* 385:79–88.
- Van Schmus W.R., and Wood J.A. (1967) A chemical-petrologic classification for the chondritic meteorites. *Geochimica et Cosmochimica Acta* 31:747-765.
- Villeneuve J., Marrocchi Y., and Jacquet E. (2020) Silicon isotopic compositions of chondrule silicates in carbonaceous chondrites and the formation of primordial solids in the accretion disk. *Earth and Planetary Science Letters* 542:116318.
- Wasson J. T., and Kallemeyn G. W. 1988. Compositions of Chondrites. *Philosophical Transactions of the Royal Society A: Mathematical, Physical and Engineering Sciences* 325:535–544.
- Yang J., and Epstein S. 1983. Interstellar organic matter in meteorites. *Geochimica et Cosmochimica Acta* 47:2199–2216.

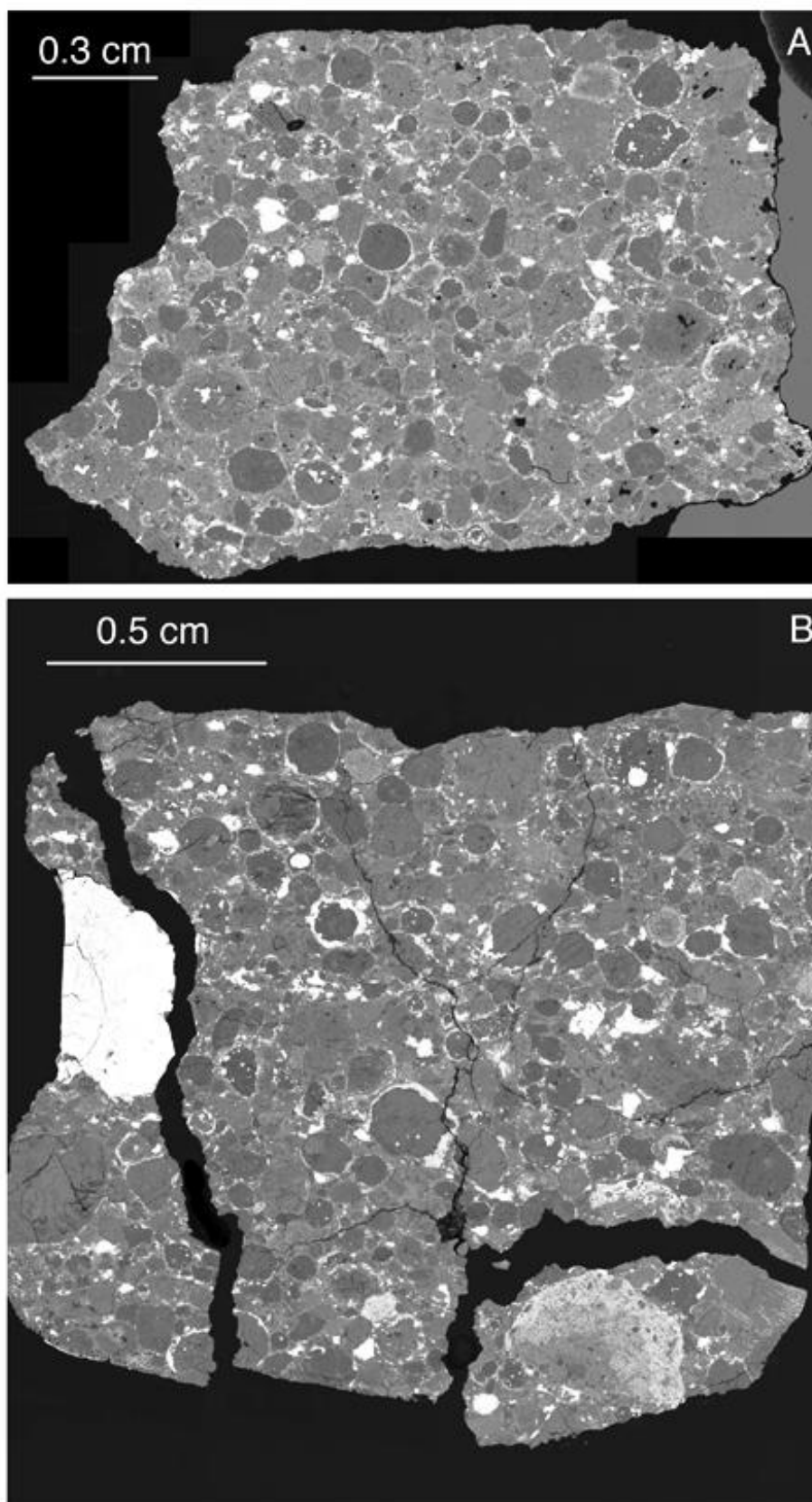
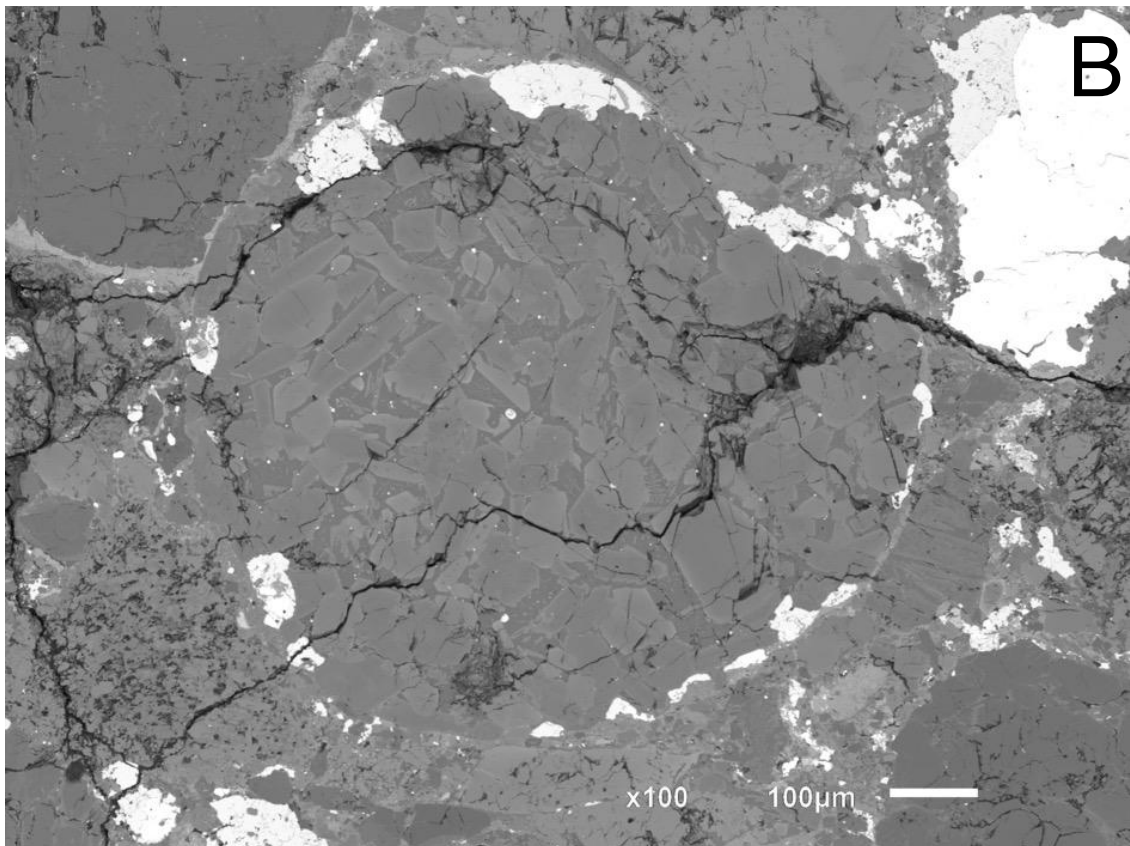
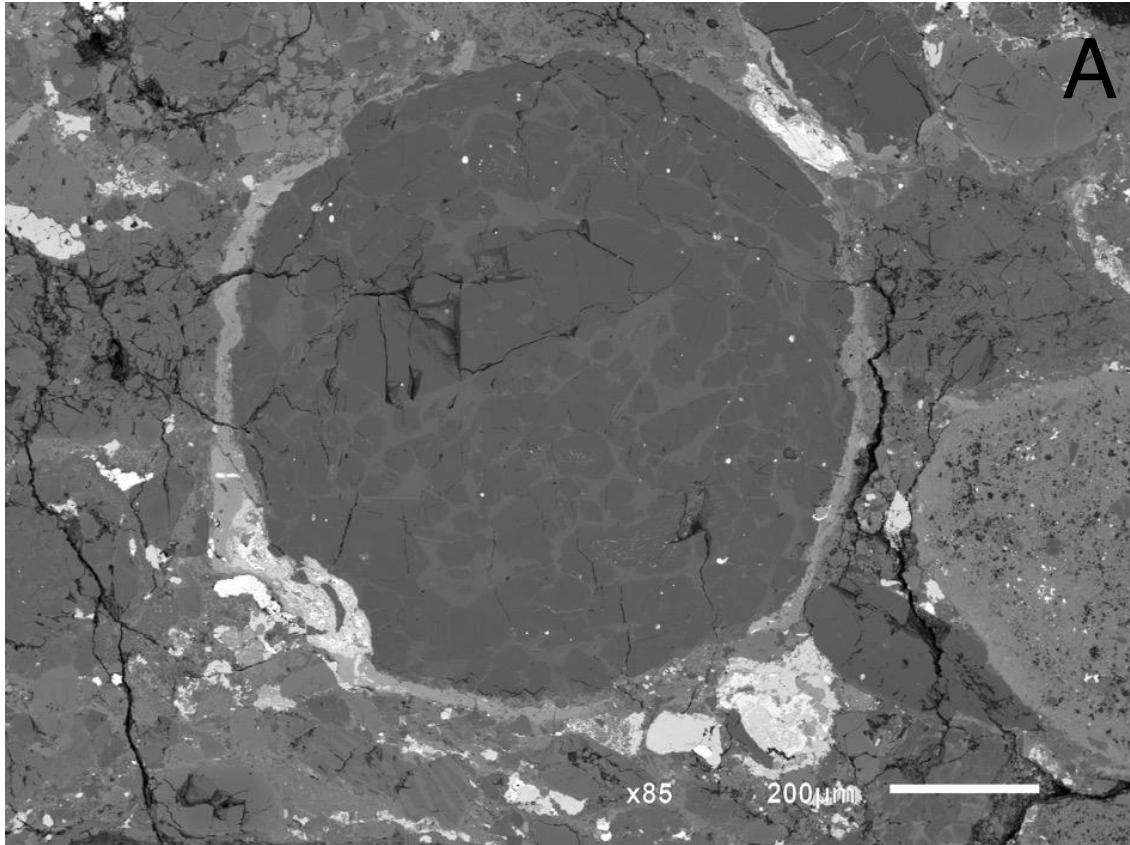


Fig. 1



644

645

Fig. 2

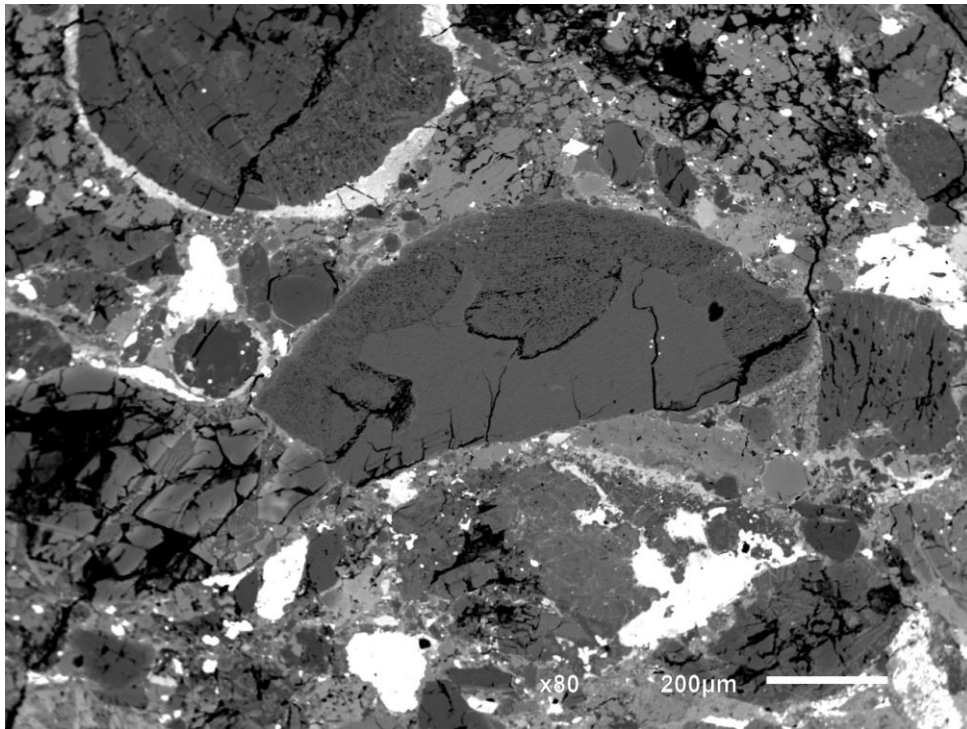


Fig. 3

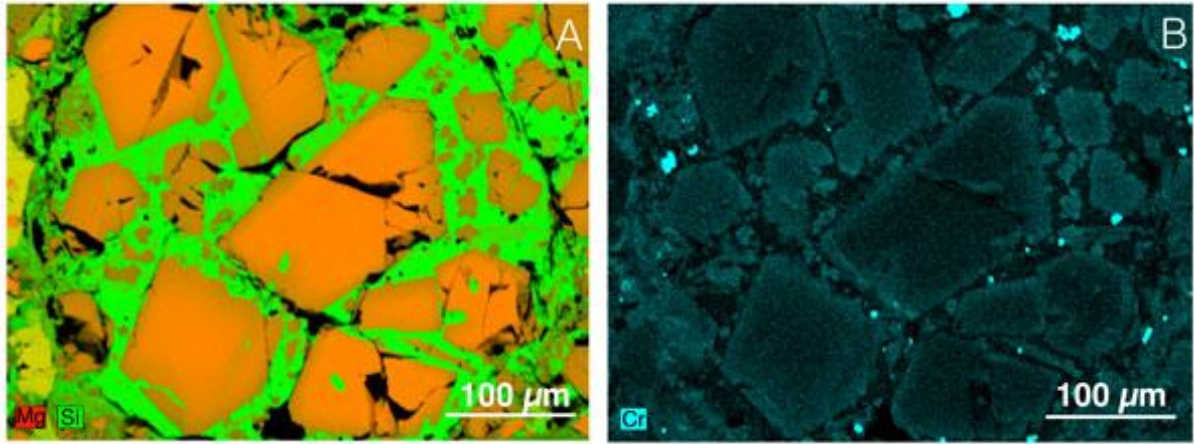
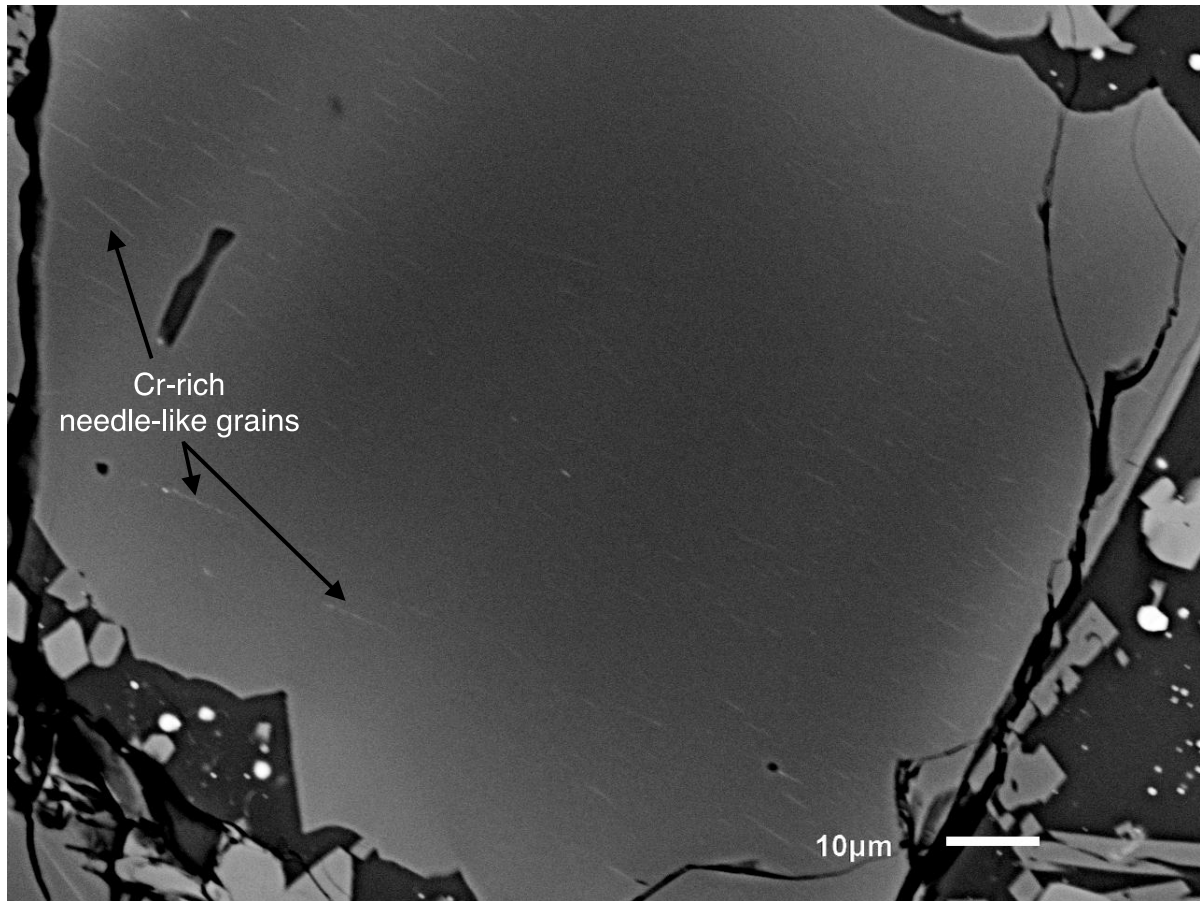


Fig. 4



663

664

Fig. 5

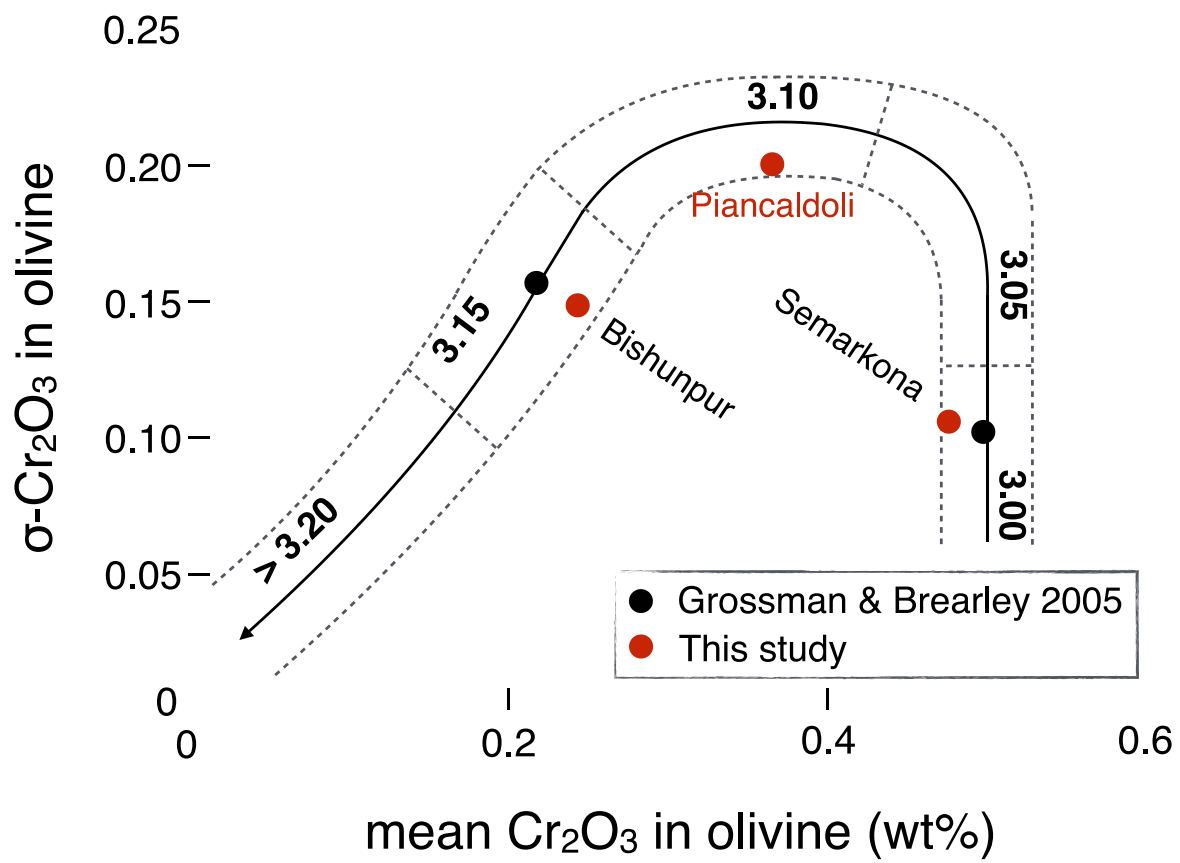


Fig. 6

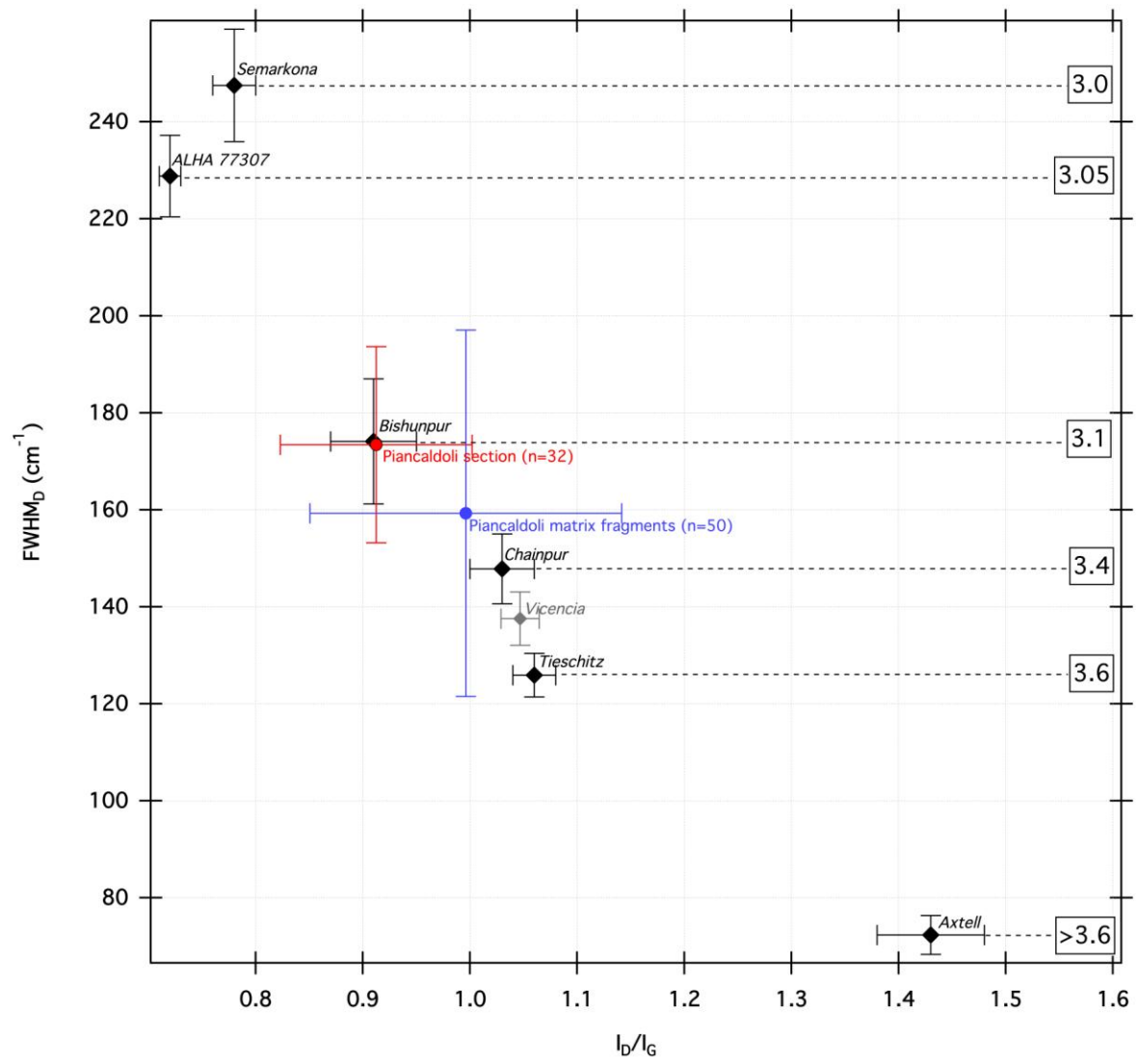


Fig. 7

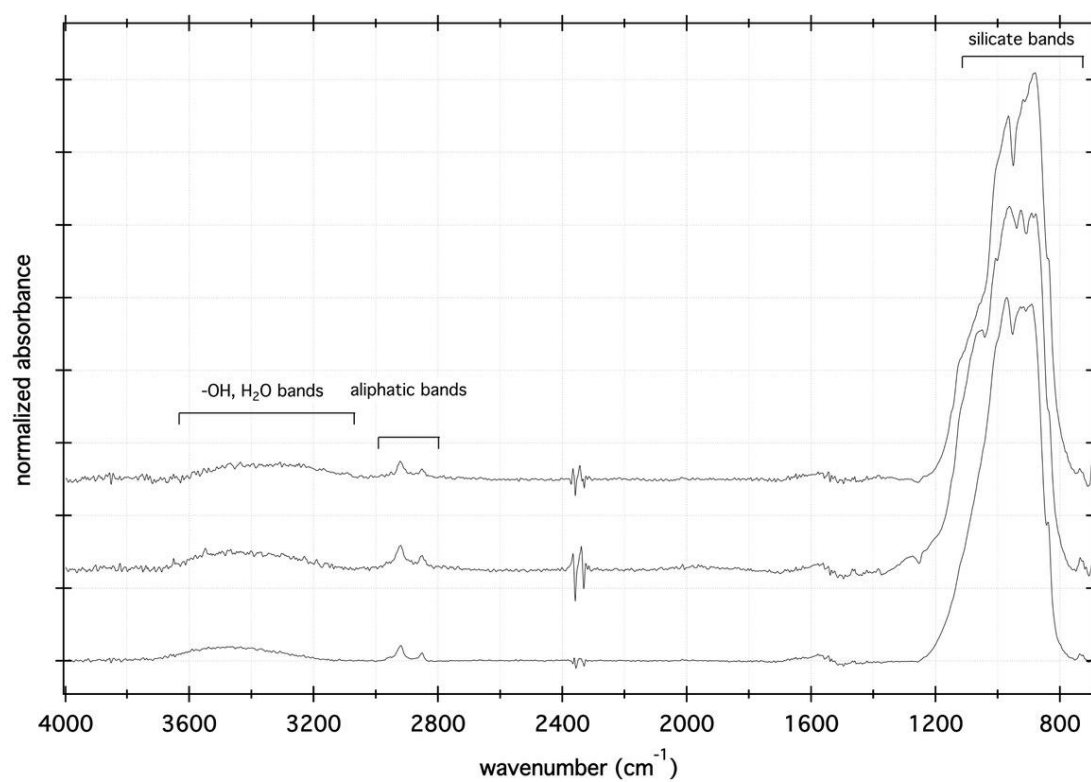


Fig. 8

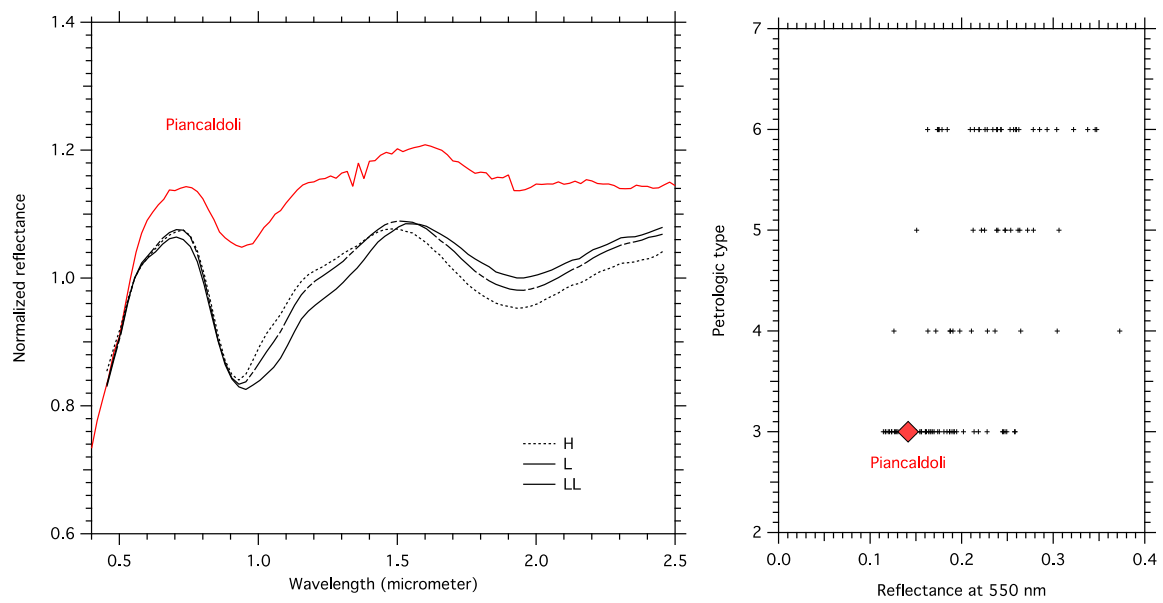


Fig. 9

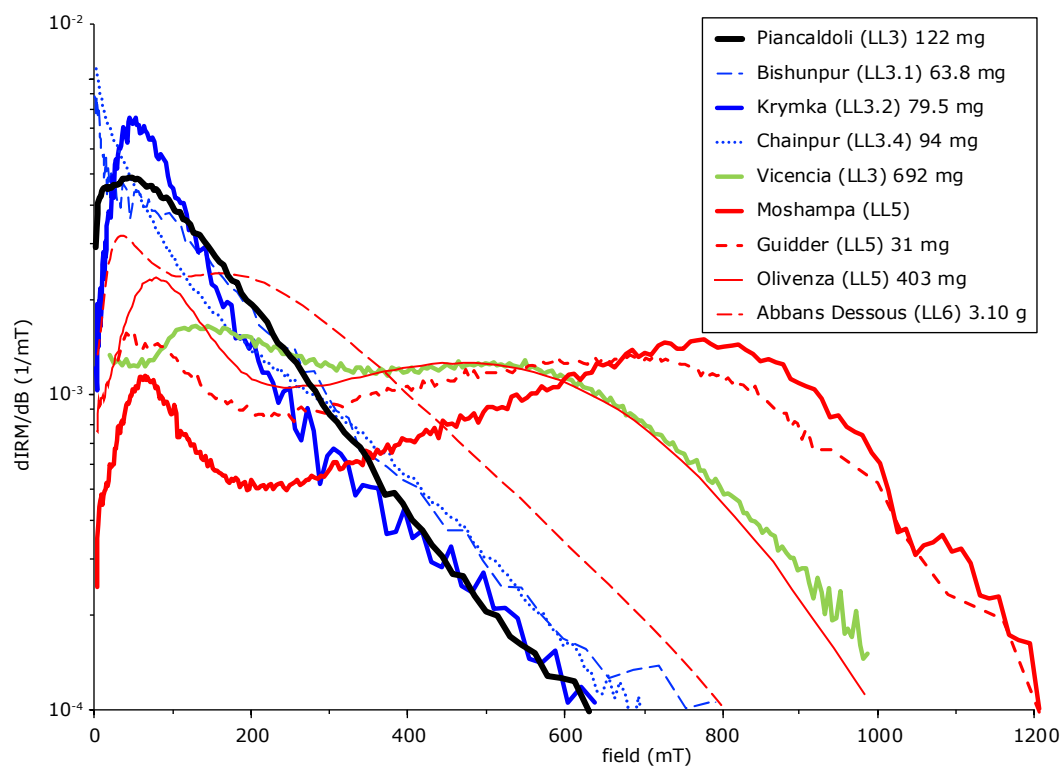


Fig. 10

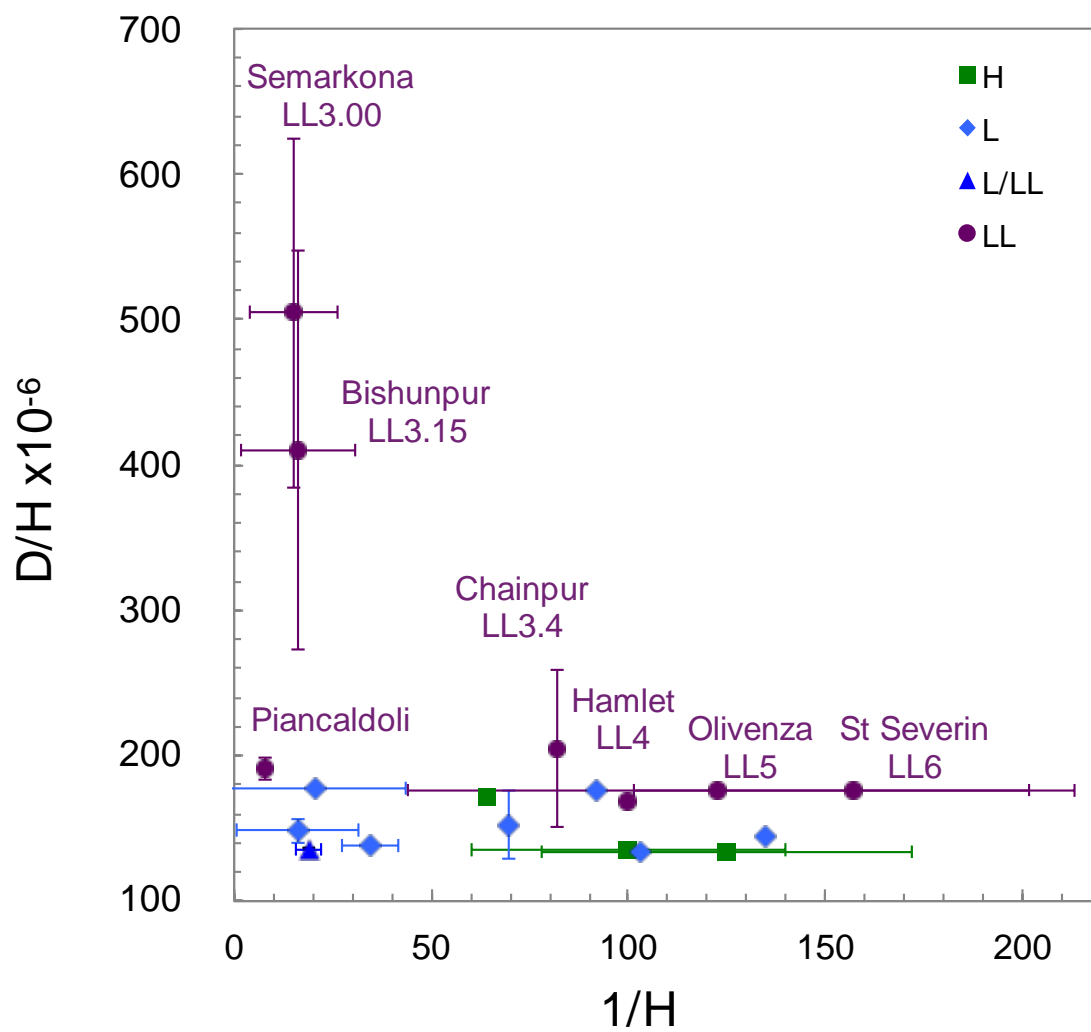


Fig. 11

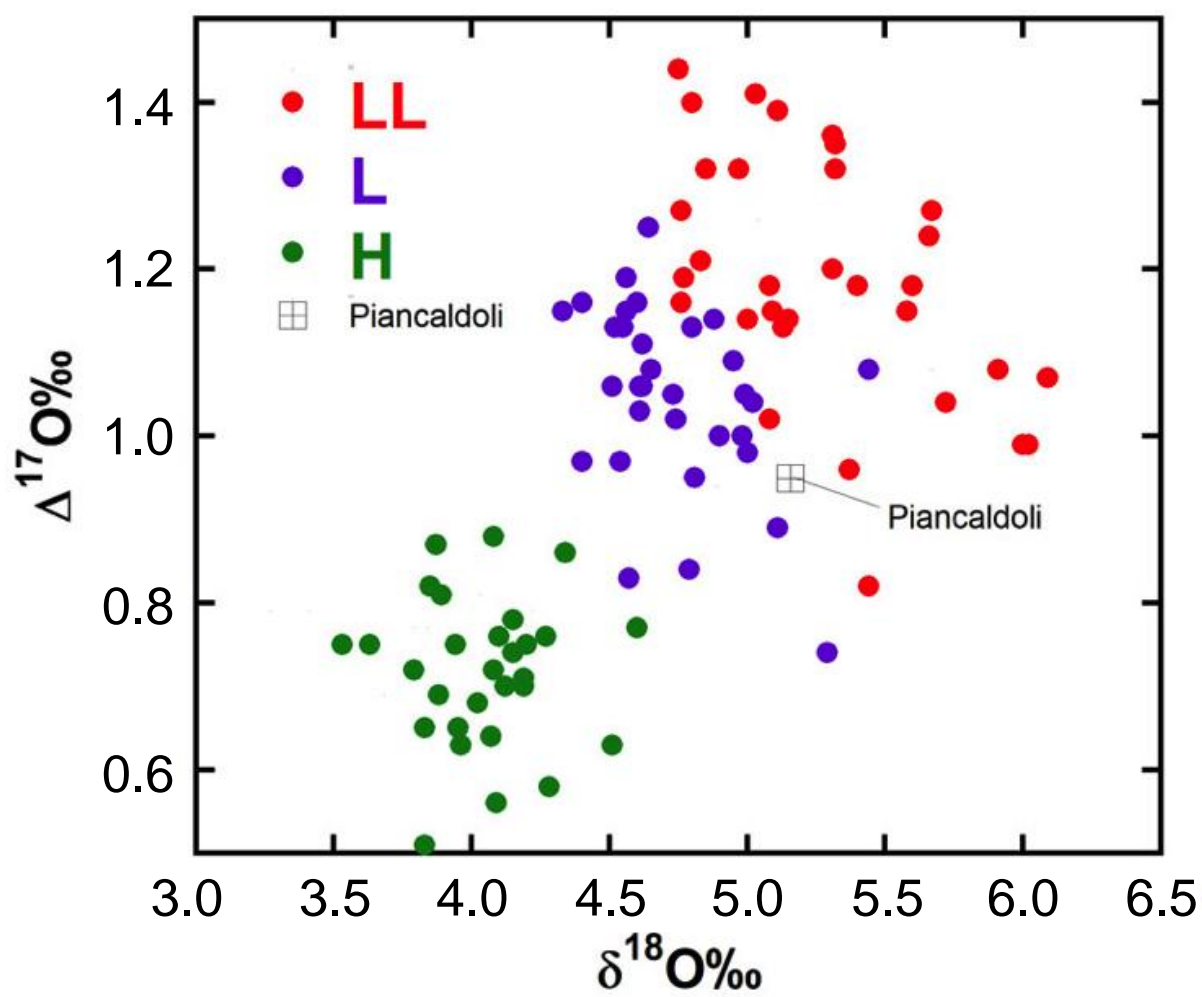


Fig. 12